Magnet Modification to Reduce Pulsating Torque for Axial Flux Permanent Magnet Synchronous Machines

Shuanglong Wu, Shuguang Zuo, Xudong Wu, Fu Lin, and Jian Shen

Clean Energy Automotive Engineering Center
Tongji University, Shanghai, 201804, China
zymwgl@foxmail.com, sgzuo@tongji.edu.cn, wuxudong@tongji.edu.cn,
linfu9.11@163.com, shenjian0821@163.com

Abstract ─ To reduce pulsating torque without sacrificing the average torque significantly in axial flux permanent magnet synchronous machines (AFPMSM), this paper presents two optimization techniques which are based on magnet modification: i) combine magnet circumferential displacement with various pole-arc ratios (method one); ii) magnet axial shape design (method two). Firstly, analytical models of air gap magnetic field were derived for the above two methods. Then, according to Maxwell stress tensor method, the analytical expressions of cogging torque and electromagnetic torque were obtained. Average torque, cogging torque and electromagnetic torque ripple were considered simultaneously in the optimization using multi-objective genetic algorithm (MOGA) with the help of the analytical torque models. Finally, 3D finite element models were established to verify the two torque optimization methods. The proposed methods were also compared with skew technique, which is widely used nowadays. Result showed that the proposed optimization techniques can greatly reduce the overall pulsating torque without decreasing the average torque and did not increase the use of permanent magnet.

Index Terms ─ Analytical model, axial flux permanent magnet synchronous machines, magnet displacement, magnet shaping, torque ripple, variable pole-arc.

I. INTRODUCTION

Compare with radial flux permanent magnet synchronous motors, axial flux permanent magnet synchronous machines (AFPMSM) have many unique characteristics such as higher power and torque density, higher efficiency and more suitable structure for installation in tight space, which have made them popular in industry [1]. However, there exists a significant amount of pulsating torque during the operation of AFPMSM, particularly at low speed and light load. Not only does this affect the control precision of the motor, it also aggravates the vibration and noise. Thus, it is necessary to optimize the torque of AFPMSM. Figure 1 depicts the typical structure of an AFPMSM. It is a 3D diagram of the 24 slots, 8 pole pairs machine with concentrated winding.

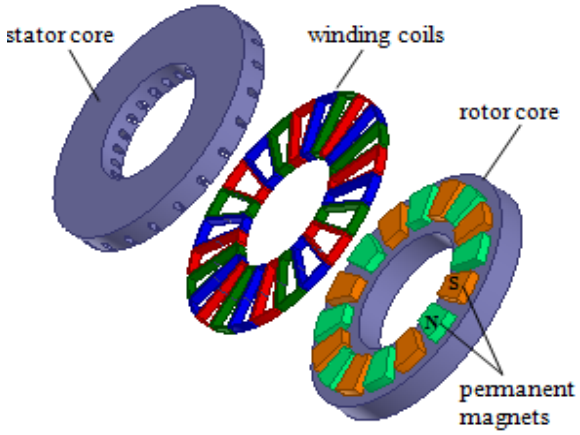

Fig. 1. 3D view of an AFPMSM.

Cogging torque and electromagnetic torque ripple are the two main sources of torque fluctuation in surface mounted AFPM motors. The former is caused by the interaction between the magnet field and stator slotting while the latter is caused by the stator magnetomotive force harmonics and PM field interaction [2]. A large amount of literatures have covered this topic. Skewing the magnets [3-6], employing various pole-arc ratios [4,7], displacing magnets or slots [4,8] and magnet shaping [9] are some of the common techniques used for reducing cogging torque. As for minimization of electromagnetic torque ripple, references [10] and [11] employ Taguchi method and rotor displacement, respectively. In [12], authors investigated the influence of skewing on cogging torque and electromagnetic torque ripple of radial flux machines. However, the optimal skew angle for reducing both the cogging torque and the electromagnetic torque ripple was not given.

Submitted On: September 30, 2015
Accepted On: February 26, 2016

From the above literatures we can see that most of the researchers concentrated on cogging torque alone or electromagnetic torque ripple alone to reduce pulsating torque in AFPMSM and few consider the two simultaneously. On the other hand, because AFPM machines have an inherent 3D electromagnetic structure, when it comes to the finite element method, time-consuming 3D FEA is always required. Therefore, it is important to establish precise analytical model to optimize the torque. References [9] and [11] pointed out that adopting those optimization methods separately such as magnet skew, rotor displacement would decrease the average torque to some extent and thus weaken the motor torque output capacity. So it is necessary to consider the average torque during the optimization and minimize its decline. We can also find that most of the torque optimization methods for AFPMSM up to now are focusing on radial and circumferential direction of the magnet. Few studied the influence of magnet axial profile on the torque. In fact, magnet shaping has already been used to optimize the torque of radial flux PM motors [13-17].

In this paper, two novel techniques for torque optimization are proposed: i) combine magnet circumferential displacement with various pole-arc ratios; ii) magnet axial shape design. Firstly, analytical models of air gap magnetic field were derived for the above two methods. Then, according to Maxwell stress tensor method the analytical expressions of cogging torque and electromagnetic torque were obtained. Average torque, cogging torque and electromagnetic torque ripple were considered simultaneously in the optimization using multi-objective genetic algorithm with the help of the analytical torque models. Finally, 3D finite element models were established to verify the two torque optimization methods. In order to further highlight the superiority of the two methods, comparison of the optimization results between the proposed methods and the skew technique which is widely used nowadays was made. Result showed that the proposed optimization techniques can greatly reduce the overall pulsating torque without decreasing the average torque and did not increase the use of permanent magnet.

II. ANALYTICAL MODEL OF AIR GAP FIELD

Assuming that the rotor and stator iron core have infinite magnetic permeability and magnetic saturation is absent, the air gap magnetic field can be obtained by linear superposition of the PM field and the armature reaction field. Thus, the analytical models of axial and tangential air gap magnetic field for the above two optimization methods can be deduced. Figure 2 shows the machine model for computing the permanent magnet field of the AFPMSM. Variable θ denotes mechanical angle in the circumferential direction along a cylindrical cutting plane of radius R at which the magnetic field is to be computed.

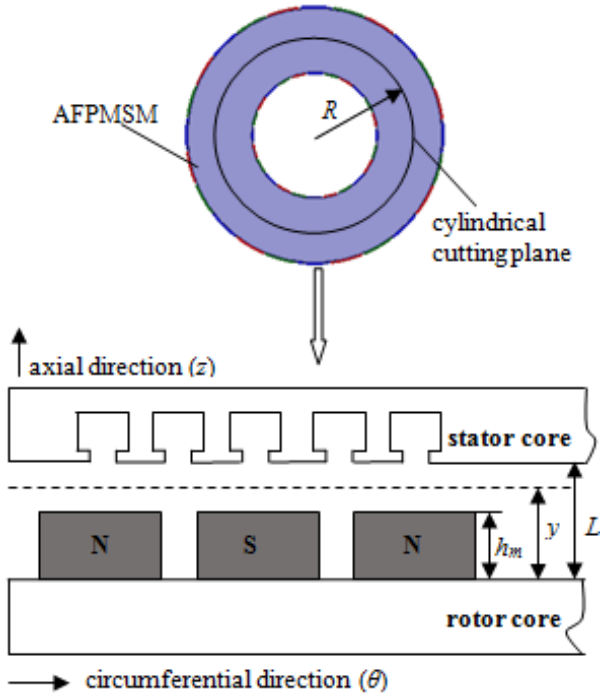

Fig. 2. Model for computation of permanent magnet field of AFPMSM.

A. Permanent magnet field

1) Permanent magnet field of method one

For conventional surface mounted AFPM machine, its magnets have the same shape with each other and are evenly arranged on the rotor surface. However, the first optimization method proposed in this paper changes the pole-arc ratio of each magnet and shifts them from their original centerline a specific angle along the rotor circumference at the same time. So the distribution of permanent magnet field changes as well. The final distribution is shown in Fig. 3. Here, assuming the pole-arc ratio and circumferential shift angle (mechanical degree) of the ith permanent magnet are α_i and d_i ($1 \le i \le 2p$), respectively.

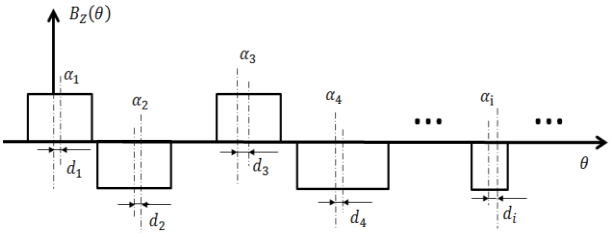

Fig. 3. Distribution of axial flux density produced by PM.

Referring to Fig. 3, the distribution of axial permanent

magnetic field can be described by a Fourier series:

$$B_{zm}(\theta,t)=\frac{a_0}{2}+a_n\cos\left[n\left(\theta-\frac{2\pi f}{p}t\right)\right]+b_n\sin\left[n\left(\theta-\frac{2\pi f}{p}t\right)\right], \quad (1)$$

where

$$\begin{cases} a_0=\dfrac{1}{\pi}\displaystyle\sum_{i=1}^{2p}\int_{-\frac{\alpha_i\pi}{2p}+d_i+\frac{(i-1)\pi}{p}}^{\frac{\alpha_i\pi}{2p}+d_i+\frac{(i-1)\pi}{p}}(-1)^{i-1}B_rK_n d\theta \\ \quad=\dfrac{2}{\pi}\displaystyle\sum_{i=1}^{2p}(-1)^{i-1}B_rK_n\frac{\alpha_i\pi}{2p} \\ a_n=\dfrac{1}{\pi}\displaystyle\sum_{i=1}^{2p}\int_{-\frac{\alpha_i\pi}{2p}+d_i+\frac{(i-1)\pi}{p}}^{\frac{\alpha_i\pi}{2p}+d_i+\frac{(i-1)\pi}{p}}(-1)^{i-1}B_rK_n\cos n\theta d\theta \\ \quad=\displaystyle\sum_{i=1}^{2p}\frac{(-1)^{i-1}B_rK_n}{n\pi}\left\{\begin{aligned}&\sin\left[n\left(\frac{\alpha_i\pi}{2p}+d_i+\frac{(i-1)\pi}{p}\right)\right]\\&-\sin\left[n\left(-\frac{\alpha_i\pi}{2p}+d_i+\frac{(i-1)\pi}{p}\right)\right]\end{aligned}\right\} \\ \quad=\displaystyle\sum_{i=1}^{2p}\frac{2(-1)^{i-1}B_rK_n}{n\pi}\cos\left[\frac{n(i-1)\pi}{p}+nd_i\right]\sin\frac{n\alpha_i\pi}{2p} \\ b_n=\dfrac{1}{\pi}\displaystyle\sum_{i=1}^{2p}\int_{-\frac{\alpha_i\pi}{2p}+d_i+\frac{(i-1)\pi}{p}}^{\frac{\alpha_i\pi}{2p}+d_i+\frac{(i-1)\pi}{p}}(-1)^{i-1}B_rK_n\sin n\theta d\theta \\ \quad\displaystyle\sum_{i=1}^{2p}\frac{(-1)^{i-1}B_rK_n}{n\pi}\left\{\begin{aligned}&-\cos\left[n\left(\frac{\alpha_i\pi}{2p}+d_i+\frac{(i-1)\pi}{p}\right)\right]\\&+\cos\left[n\left(-\frac{\alpha_i\pi}{2p}+d_i+\frac{(i-1)\pi}{p}\right)\right]\end{aligned}\right\} \\ \quad\displaystyle\sum_{i=1}^{2p}\frac{2(-1)^{i-1}B_rK_n}{n\pi}\sin\left[\frac{n(i-1)\pi}{p}+nd_i\right]\sin\frac{n\alpha_i\pi}{2p}, \end{cases} \quad (2)$$

and θ is the mechanical angle, t is the time, n is the order of magnetic field harmonics, f is the current frequency, Br is the remanent flux density, p is the number of pole pairs, K_n is the correction factor which can be found in [18];

$$K_n=\frac{\sinh\left(\frac{n\pi h_m}{\tau_p p}\right)\cosh\left[\frac{n\pi(L-y)}{\tau_p p}\right]}{\Delta}, \quad (3)$$

where

$$\begin{aligned}\Delta=&\mu_r\cosh\left(\frac{n\pi h_m}{\tau_p p}\right)\sinh\left[\frac{n\pi(L-h_m)}{\tau_p p}\right]\\&+\cosh\left(\frac{n\pi(L-h_m)}{\tau_p p}\right)\sinh\left[\frac{n\pi h_m}{\tau_p p}\right],\end{aligned} \quad (4)$$

μ_r is the relative permeability, h_m is the axial thickness of magnets, L is the axial distance between inner surfaces of the rotor and stator, y is the axial distance between rotor inner surface and the axial air gap plane at which field is computed, $\tau_p=\pi R/p$ is the pole pitch in circumferential direction and R is the radius of cutting plane at which field is computed.

Substituting (2) and (3) into (1), the axial component of permanent magnet field in air region of a AFPMSM is:

$$\begin{aligned}B_{zm}(\theta,t)=&\frac{K_nB_r}{\pi}\sum_{i=1}^{2p}\frac{(-1)^{i-1}\alpha_i\pi}{2p}+K_nB_r\\&\times\sum_{n=1}^{\infty}\left\{\begin{aligned}&\sum_{i=1}^{2p}\frac{2}{n\pi}(-1)^{i-1}\cos\left[\frac{n(i-1)\pi}{p}+nd_i\right]\\&\times\sin\frac{n\alpha_i\pi}{2p}\cos\left[n\left(\theta-\frac{2\pi f}{p}t\right)\right]\\&+\sum_{i=1}^{2p}\frac{2}{n\pi}(-1)^{i-1}\sin\left[\frac{n(i-1)\pi}{p}+nd_i\right]\\&\times\sin\frac{n\alpha_i\pi}{2p}\sin\left[n\left(\theta-\frac{2\pi f}{p}t\right)\right]\end{aligned}\right\}.\end{aligned} \quad (5)$$

Similarly, the circumferential component of permanent magnetic field can be obtained as follows:

$$\begin{aligned}B_{\theta m}(\theta,t)=&K_n^*B_r\\&\times\sum_{n=1}^{\infty}\left\{\begin{aligned}&\sum_{i=1}^{2p}\frac{2}{n\pi}(-1)^{i-1}\sin\left[\frac{n(i-1)\pi}{p}+nd_i\right]\\&\times\sin\frac{n\alpha_i\pi}{2p}\cos\left[n\left(\theta-\frac{2\pi f}{p}t\right)\right]\\&-\sum_{i=1}^{2p}\frac{2}{n\pi}(-1)^{i-1}\cos\left[\frac{n(i-1)\pi}{p}+nd_i\right]\\&\times\sin\frac{n\alpha_i\pi}{2p}\sin\left[n\left(\theta-\frac{2\pi f}{p}t\right)\right]\end{aligned}\right\},\end{aligned} \quad (6)$$

where

$$K_n^*=K_n\tanh\left[\frac{n\pi(L-y)}{\tau_p p}\right]. \quad (7)$$

The above analytical expressions of permanent magnetic field contain a total of $4p$ variables α_i and d_i ($1\le i\le 2p$). By choosing different values, we can obtain the magnetic field distribution in the air region under magnets circumferential displacement and employing various pole-arc ratios simultaneously.

2) Permanent magnet field of method two

Divide each piece of the permanent magnets along with the circumferential direction into $N=2k+1$ ($k=0,1,2,3\cdots$) segments with the same arc and each segment can have independent value in thickness as shown in Fig. 4. Theoretically, with the increase of subsection number N, it can approximate any permanent magnet with random axial profile.

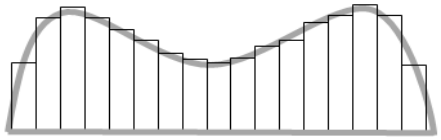

Fig. 4. Segmented permanent magnet.

As for the magnetic field produced by those segmented permanent magnet, we can first derive the field of each segment and then add all of the N sections

to obtain the field of one pole. Finally, by array transformation of the single pole field along with the circumferential direction, the analytical model of the rotor permanent magnetic field is established. The axial and circumferential component of magnetic field of the first segment can be expressed as follows:

$$\begin{cases} B_{zm1}(\theta,t) = B_0 + \sum_{\mu}\left[B_{z_1\mu}\cos(\mu\theta-\mu\omega_r t) + B_{z_2\mu}\sin(\mu\theta-\mu\omega_r t)\right] \\ B_{\theta m1}(\theta,t) = \sum_{\mu}\left[B_{\theta_1\mu}\cos(\mu\theta-\mu\omega_r t) - B_{\theta_2\mu}\sin(\mu\theta-\mu\omega_r t)\right], \end{cases} \tag{8}$$

where θ is the mechanical angle, t is the time, μ is the order of magnetic field harmonics, ω_r is the rotor angular velocity. The coefficients in (8) can be obtained as follows:

$$\begin{cases} B_0 = \dfrac{1}{2\pi}\int_{-\pi}^{\pi} B_{zm1}(\theta)\,d\theta \\ \quad = \dfrac{1}{2\pi}\sum\limits_{i=\frac{N-1}{2}}^{\frac{1-N}{2}}\left[\int_{-\frac{\alpha_p\pi}{2pN}-\frac{\alpha_p\pi i}{pN}}^{\frac{\alpha_p\pi}{2pN}-\frac{\alpha_p\pi i}{pN}} B_r\times\dfrac{h_m(i)}{h_m(i)+\delta(i)\mu_r}\,d\theta\right] \\ \quad = \dfrac{\alpha_p}{pN}\sum\limits_{i=\frac{N-1}{2}}^{\frac{1-N}{2}}\left[B_r\times\dfrac{h_m(i)}{h_m(i)+\delta(i)\mu_r}\right] \\ B_{z_1\mu} = \dfrac{1}{\pi}\int_0^{2\pi} B_{zm1}(\theta)\cos(\mu\theta)\,d\theta \\ \quad = \dfrac{1}{\pi}\sum\limits_{i=\frac{N-1}{2}}^{\frac{1-N}{2}}\left[\int_{-\frac{\alpha_p\pi}{2pN}-\frac{\alpha_p\pi i}{pN}}^{\frac{\alpha_p\pi}{2pN}-\frac{\alpha_p\pi i}{pN}} B_r K_\mu(i)\cos\mu\theta\,d\theta\right] \\ \quad = \sum\limits_{i=\frac{N-1}{2}}^{\frac{1-N}{2}}\dfrac{2}{\mu\pi}B_r K_\mu(i)\cos\dfrac{\alpha_p\mu\pi i}{pN}\sin\dfrac{\alpha_p\mu\pi}{2pN} \\ B_{z_2\mu} = \dfrac{1}{\pi}\int_0^{2\pi} B_{zm1}(\theta)\sin(\mu\theta)\,d\theta \\ \quad = \dfrac{1}{\pi}\sum\limits_{i=\frac{N-1}{2}}^{\frac{1-N}{2}}\left[\int_{-\frac{\alpha_p\pi}{2pN}-\frac{\alpha_p\pi i}{pN}}^{\frac{\alpha_p\pi}{2pN}-\frac{\alpha_p\pi i}{pN}} B_r K_\mu(i)\sin\mu\theta\,d\theta\right] \\ \quad = \sum\limits_{i=\frac{N-1}{2}}^{\frac{1-N}{2}}\dfrac{2}{\mu\pi}B_r K_\mu(i)\sin\dfrac{\alpha_p\mu\pi i}{pN}\sin\dfrac{\alpha_p\mu\pi}{2pN} \\ B_{\theta_1\mu} = B_{z_2\mu}\times\tanh\left[\dfrac{\mu\delta(i)}{2R}\right] \\ B_{\theta_2\mu} = B_{z_1\mu}\times\tanh\left[\dfrac{\mu\delta(i)}{2R}\right], \end{cases} \tag{9}$$

where $h_m(i)$ ($1\le i\le N$) is the thickness of the ith segment, α_p is the pole-arc ratio of one pole, $\delta(i)=h_m+g-h_m(i)$ is the real air gap length of the ith segment, h_m is the initial thickness of the permanent magnet and g is the initial air gap length, $K_\mu(i)$ is the correction factor of the ith segment [18];

$$K_\mu(i) = \frac{\sinh\left[\dfrac{\mu\pi h_m(i)}{\tau_p p}\right]\cosh\left[\dfrac{\mu\pi(L-y)}{\tau_p p}\right]}{\Delta'}, \tag{10}$$

where

$$\begin{aligned}\Delta' = \mu_r\cosh\left[\frac{\mu\pi h_m(i)}{\tau_p p}\right]\sinh\left\{\frac{\mu\pi\left[L-h_m(i)\right]}{\tau_p p}\right\} \\ +\cosh\left\{\frac{\mu\pi\left[L-h_m(i)\right]}{\tau_p p}\right\}\sinh\left[\frac{\mu\pi h_m(i)}{\tau_p p}\right].\end{aligned} \tag{11}$$

Based on the above derivation, the analytical model of the rotor permanent magnetic field can be established eventually by array transformation of the single pole field along with the circumferential direction;

$$\begin{cases} B_{zm}(\theta,t) = \sum\limits_{j=1}^{2p} B_{zmj}(\theta,t) = \sum\limits_{j=1}^{2p}(-1)^{j-1}B_{mz1}\left[\theta-\dfrac{(j-1)\pi}{p},t\right] \\ B_{\theta m}(\theta,t) = \sum\limits_{j=1}^{2p} B_{\theta mj}(\theta,t) = \sum\limits_{j=1}^{2p}(-1)^{j-1}B_{m\theta 1}\left[\theta-\dfrac{(j-1)\pi}{p},t\right], \end{cases} \tag{12}$$

where $B_{zmj}(\theta, t)$ and $B_{\theta mj}(\theta, t)$ are axial and circumferential component of the magnetic field produced by the jst magnet pole, $j(1\le j\le 2p)$ represents the serial number of $2p$ poles.

B. Armature reaction field

The axial flux permanent magnet motors with one rotor and one stator often use the drum winding. While neglecting the current harmonics, the axial and circumferential components of armature reaction field can be obtained as follows [19]:

$$B_{za}(\theta,t) = \frac{4\mu_0 N_c i}{\pi}\sum_{v}\frac{k_{pn}k_{son}}{v\sinh\dfrac{vy_1}{R}}\cosh\frac{vy}{R}\cos\left[v(\theta\pm 2\pi ft)\right], \tag{13}$$

$$B_{\theta a}(\theta,t) = -\frac{4\mu_0 N_c i}{\pi}\sum_{v}\frac{k_{pn}k_{son}}{v\sinh\dfrac{vy_1}{R}}\sinh\frac{vy}{R}\sin\left[v(\theta\pm 2\pi ft)\right], \tag{14}$$

where v is the order of armature reaction field harmonics, μ_0 is the permeability of vacuum, N_{ci} is the ampere-turns of the coil, k_{pn} is the coil pitch factor, k_{son} is the slot opening factor, $y_1=h_m+g$ is the axial distance between the inner surfaces of the rotor and stator.

C. Relative permeance

Slotting will affect the distribution of the flux in the air gap and its effect can be accounted by introducing the relative permeance;

$$\lambda(\theta) = \lambda_0 + \sum_k \lambda_k\cos(kQ_s\theta), \tag{15}$$

where k is the order of the relative permeance harmonics, Q_s is the number of stator teeth, λ_0 is the mean permeance and λ_k is the peak value of the kst harmonic which can be found in [20].

D. Air gap resultant magnetic field

Assuming that the stator and rotor cores are nonsaturated, the air gap resultant magnetic field can be obtained by linear superposition of the PM field and the armature reaction field, while the relative permeance is introduced to account for the effect of slotting;

$$\begin{cases} B_z(\theta,t)=\left[B_{zm}(\theta,t)+B_{za}(\theta,t)\right]\cdot\lambda(\theta) \\ B_\theta(\theta,t)=\left[B_{\theta m}(\theta,t)+B_{\theta a}(\theta,t)\right]\cdot\lambda(\theta). \end{cases} \quad (16)$$

III. ANALYTICAL MODEL OF TORQUE

Torque can be calculated based on double integral of the circumferential component of magnetic force. And the force is obtained by using Maxwell stress tensor method [21];

$$T_{cog}=\int_0^{2\pi}\int_{R_i}^{R_o} f_{\theta 1}drd\theta=\int_0^{2\pi}\int_{R_i}^{R_o}\frac{B_{mz}B_{m\theta}\lambda_a^2}{\mu_0}drd\theta, \quad (17)$$

$$T_{ele}=\int_0^{2\pi}\int_{R_i}^{R_o} f_{\theta 2}drd\theta=\int_0^{2\pi}\int_{R_i}^{R_o}\frac{(B_{mz}+B_{az})\times(B_{m\theta}+B_{a\theta})}{\mu_0}drd\theta, \quad (18)$$

where T_{cog} and T_{ele} represent cogging torque and electromagnetic torque respectively, $f_{\theta 1}$ and $f_{\theta 2}$ are the circumferential component of magnetic force on no-load and load respectively, R_i is inner and R_o is outer radius of the permanent magnet.

IV. TORQUE OPTIMIZATION USING MULTI-OBJECTIVE GENETIC ALGORITHM

As for the assessment of motor torque fluctuation, the torque ripple factor (*TRF*) is often used to describe the electromagnetic torque ripple, while the peak to peak value (T_{cPP}) is used for cogging torque [22];

$$\begin{cases} TRF=\dfrac{T_{ripple}}{T_{average}}=\dfrac{2\sqrt{\sum_i T_i^2}}{T_{average}} \\ T_{cPP}=\max(T_{cog})-\min(T_{cog}), \end{cases} \quad (19)$$

where T_{ripple} is the electromagnetic torque ripple, $T_{average}$ is the average torque, T_i is the *i*st time harmonic peak value of the electromagnetic torque ripple.

A. Method one

Based on the analytical expressions of (5), (6), (17), (18), and using the multi-objective genetic algorithm, we can obtain the optimal values of shift angle and pole-arc ratio of each magnet on the premise of suppressing the overall pulsating torque greatly without decreasing the average torque.

1) Optimization objectives

According to the assessment criteria in (19), the first optimization goal *Obj1* is set to maximize the average torque and the second goal *Obj2* is set to minimize the summation of the electromagnetic torque ripple and cogging torque;

$$\begin{cases} Obj1=\max(T_{average}) \\ Obj2=\min\left(T_{ripple}+T_{cPP}\right)=\min\left[\sqrt{\sum_i T_i^2}+\dfrac{\max(T_{cog})-\min(T_{cog})}{2}\right], \end{cases} \quad (20)$$

where $T_{average}$ is the average torque, T_{cog} is the cogging torque, T_i is the *i*st time harmonic peak value of the electromagnetic torque ripple. The original values of *Obj1* and *Obj2* of the virtual prototype studied in this paper before optimization are 57.71 Nm and 7.8 Nm, respectively.

2) Constraints

(a). In order to ensure that any two adjacent permanent magnets do not touch each other after optimization, the shift angle and pole-arc ratio of each magnet should be satisfied:

$$d_{i+1}-d_i<\frac{180}{p}\left(1-\frac{\alpha_{i+1}}{2}-\frac{\alpha_i}{2}\right). \quad (21)$$

(b). Considering the cost, the amount of permanent magnet should remain the same before and after optimization:

$$\sum_{i=1}^{2p}\alpha_i=2p\alpha_p, \quad (22)$$

where α_p is the pole-arc ratio before optimization.

(c). The pole-arc ratio of each magnet after optimization should be satisfied:

$$0<\alpha_i<1. \quad (23)$$

(d). In order to keep the symmetry of the magnetic circuit so as not to produce additional unbalanced magnetic pull and overturning moment after optimization, the shift angle and pole-arc ratio of the two magnets which locate on diametrically opposed position should have the same value. Therefore, for $1<i<p$, we have:

$$\begin{cases} \alpha_i=\alpha_{i+p} \\ d_i=d_{i+p}. \end{cases} \quad (24)$$

3) Optimization variables and parameters of virtual prototype

From the last constraint above we can conclude that although method one contains a total of $4p$ variables α_i and d_i ($1\le i\le 2p$), only half of them are independent. Now we will use this method to optimize the torque of a 16P24S AFPMSM with one stator and one rotor under the rated conditions. The initial parameters of the virtual prototype are listed in Table 1. The average torque before optimization is 57.71 Nm. The amplitude of electromagnetic torque ripple under the rated conditions and cogging torque under no load are 4.71 Nm and 3.13 Nm, respectively.

Table 1: Initial parameters of virtual prototype

Parameter	Value	Parameter	Value
Pole pairs	8	Slot number	24
PM thickness	7.5 mm	Remanence	1.1 T
Air gap length	2 mm	Rotor thickness	15 mm
Outer diameter of PM	89 mm	Inner diameter of PM	55.7 mm
Pole-arc ratio	0.6	Phase number	3
Slot width	8 mm	Coil turns	148
Current frequency	100 Hz	Current amplitude	72.4 A

4) Optimized result

The optimization was accomplished by using the multi-objective genetic algorithm. Here the population size is set to 240 and the creation function is constraint dependent. The selection model is tournament selection and the tournament size is 2. After 352 generations while the function tolerance is 0.0001, a subset of Pareto optimal solutions is obtained as shown in Fig. 5. Then select the optimal value of these variables according to the criteria that average torque remains the same as far as possible before and after optimization (in black circle). The final values of those variables are listed in Table 2. From Fig. 5 we can see that the overall pulsating torque was suppressed greatly while the average torque did not decline.

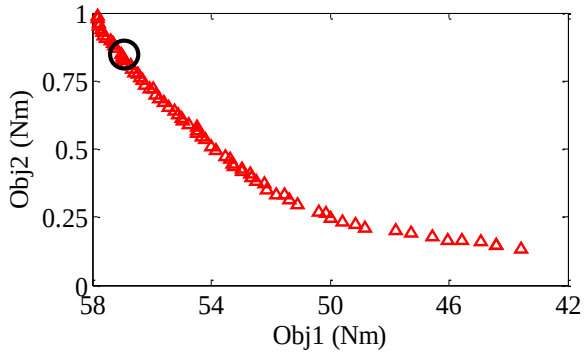

Fig. 5. Pareto optimal solutions set of method one.

Table 2: Variable-value of method one

Variable	Value	Variable	Value
$\alpha_1\ \alpha_9$	0.41	$\delta_1\ \delta_9$	0°
$\alpha_2\ \alpha_{10}$	0.56	$\delta_2\ \delta_{10}$	-1.84°
$\alpha_3\ \alpha_{11}$	0.84	$\delta_3\ \delta_{11}$	-1.89°
$\alpha_4\ \alpha_{12}$	0.43	$\delta_4\ \delta_{12}$	0.69°
$\alpha_5\ \alpha_{13}$	0.77	$\delta_5\ \delta_{13}$	1.41°
$\alpha_6\ \alpha_{14}$	0.63	$\delta_6\ \delta_{14}$	4.30°
$\alpha_7\ \alpha_{15}$	0.42	$\delta_7\ \delta_{15}$	1.63°
$\alpha_8\ \alpha_{16}$	0.76	$\delta_8\ \delta_{16}$	-1.53°

B. Method two

Based on the analytical expressions of (12), (17), (18), and using the multi-objective genetic algorithm, we can obtain the optimal values of each segment permanent magnet thickness on the premise of suppressing the overall pulsating torque greatly without decreasing the average torque.

5) Optimization objectives

For comparison, the optimization objectives used in method two are the same as those in method one, as shown in (20).

6) Constraints

(a). Due to the motor air gap length is generally small and considering the manufacturing and assembly error, keeping the maximum thickness of permanent magnet unchanged before and after optimization:

$$max\left[h_m(i)\right]=h_m, 1\le i\le N. \tag{25}$$

(b). In order to keep the symmetry of the magnetic circuit, each permanent magnet should be symmetrical about its centerline:

$$h_m(i)=h_m(N-i+1). \tag{26}$$

(c). From the first constraint we know that the amount of permanent magnet will be reduced after optimization. So we should increase the pole-arc ratio to compensate for the reduction:

$$\frac{\alpha_p^*}{N}\sum_{i=1}^{N}h_m(i)=\alpha_p h_m, \tag{27}$$

where α_p^* is the pole-arc ratio after optimization.

(d). The pole-arc ratio of each magnet after optimization should be satisfied:

$$0<\alpha_p^*<1. \tag{28}$$

7) Optimization variables and parameters of virtual prototype

The optimization variables of method two are those thickness values of each segment permanent magnet. The optimization object is the same virtual prototype used in method one. The initial parameters of the virtual prototype are listed in Table 1.

8) Optimized result

Theoretically, with the increase of subsection number *N*, it can reflect the continuous variation of permanent magnet outline truly but the optimization iteration time will be longer. In order to determine the optimal value of *N*, we get the subset of Pareto optimal solutions for different *N*, as shown in Fig. 6.

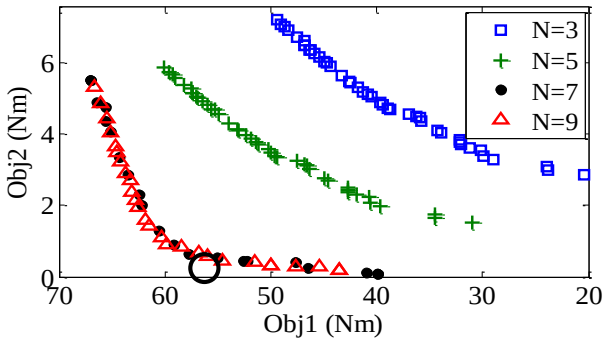

Fig. 6. Pareto optimal solutions set of method two.

We can see that when $N\ge7$, the subset of Pareto optimal solutions overlaps with each other. Continue to

increase the subsection number will only increase the iteration time but not the optimization precision. So we finally chose N=9. During the optimization, the population size is set to 110 and the creation function is constraint dependent. The selection model is tournament selection and the tournament size is 2. It takes 286 generations to get the result as shown in Fig. 6, while the function tolerance is 0.0001. Similarly, select the optimal value of these variables according to the criteria that average torque remains the same as far as possible before and after optimization (in black circle). The final values of those variables are listed in Table 3. The pole-arc ratio after optimization is 0.71.

Table 3: Variable-value of method two

i	$h_m(i)$	i	$h_m(i)$
1	6.50 mm	6	7.10 mm
2	5.13 mm	7	6.00 mm
3	6.00 mm	8	5.13 mm
4	7.10 mm	9	6.50 mm
5	7.50 mm		

Based on the data in Table 3, the permanent magnet axial profile curve after optimization is obtained (as shown in Fig. 7) using polynomial fit technique:

$$h_m(i) = h_m \times \left(p_1 x^4 + p_2 x^3 + p_3 x^2 + p_4 x + p_5 \right), \quad (29)$$

where x=0.5×[N^*/N(2i-1)+1] (1≤i≤N^*), N^*=9 is the subsection number in optimization, N is the subsection number in polynomial fit. p_i=[3.855,-77.1,507.3,-1217,1644]×10^{-3} is the coefficient.

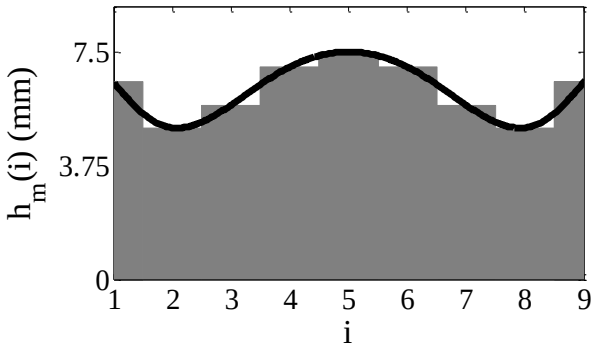

Fig. 7. Permanent magnet axial profile curve.

V. VERIFICATION BY 3D FEM AND RESULTS CONTRAST

According to the two optimization results above, we obtained the corresponding optimized motor models by modifying the initial rotor structure of the virtual prototype as shown in Figs. 8 (a) and (b). On the left side of both Figs. 8 (a) and (b) are the 3D finite element model. The AFPM machine is surrounded by the blue transparent solution region which is generated by the software automatically. On the right side are rotors with optimized permanent magnets.

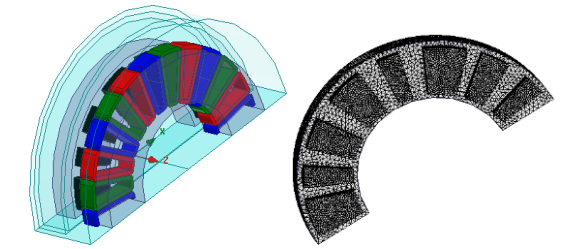

(a) Method one

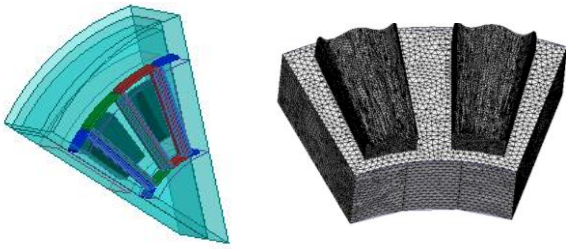

(b) Method two

Fig. 8. 3D finite element model of the optimized AFPMSM.

A. Verification of the proposed method by 3D FEM

As for method one, the pole-arc ratio of each magnet has been changed but the two magnets which locate on diametrically opposed position have the same pole-arc ratio. By taking advantage of machine symmetry, only one half of the machine is considered as shown in Fig. 8 (a). For method two, since each permanent magnet has the same shape and evenly arranged on the rotor surface, only 1/8 of the machine is needed as shown in Fig. 8 (b).

To verify the accuracy of the analytical models, the electromagnetic torque and cogging torque were computed using both the FEM and analytical method. In addition, the comparison of torque value between optimized models and initial model is also made to verify the validity of the two proposed methods. The results are shown in Fig. 9 and Fig. 10.

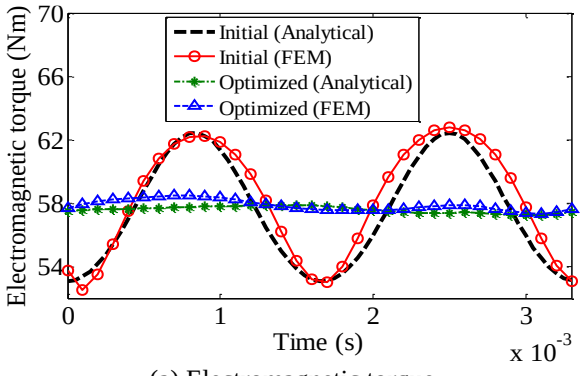

(a) Electromagnetic torque

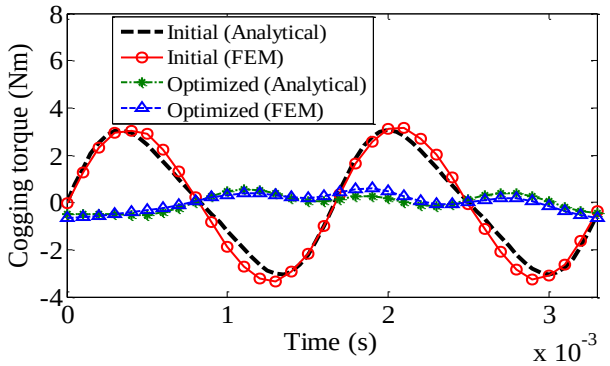

(b) Cogging torque

Fig. 9. Torque contrast before and after optimization of method one.

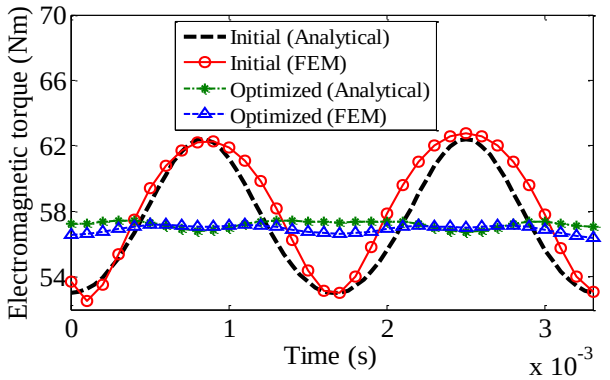

(a) Electromagnetic torque

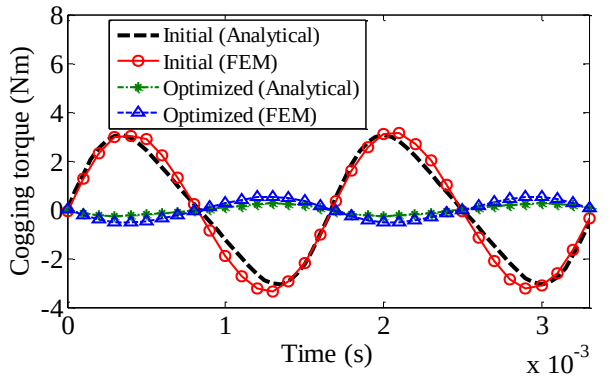

(b) Cogging torque

Fig. 10. Torque contrast before and after optimization of method two.

Good agreement between the analytical result and FEA result confirms the accuracy of the analytical models. On the other hand, we can also see that the overall pulsating torque was suppressed greatly while the average torque almost did not decline after optimization. So the validity of the two proposed methods is verified.

B. Optimization results comparison

In order to further highlight the superiority of the two methods, comparison of the optimization results between the proposed methods and the skew technique is made. After all, skew technique is one of the most effective torque optimization methods which is popular nowadays [2-4].

Similarly, the analytical models of electromagnetic torque and cogging torque for AFPMSM with skew magnets can be derived. Figure 11 shows the variation of the torque relative value waveform of the same virtual prototype as the skew angle is varied. As shown, when the skew angle is 60 electrical degrees, the electromagnetic torque ripple and cogging torque are greatly weakened while the average torque is only a slight decline.

Figure 12 is the 3D finite element model of the same virtual prototype with magnets skewing 60 electrical degrees. The electromagnetic torque and cogging torque were computed using the FEM and compared with those obtained by the two proposed methods as shown in the Fig. 13. It is obvious that not only the skew method is inferior to the two proposed methods in suppressing the pulsating torque, it will also decrease the average torque and thus weaken the motor torque output capacity. For the convenience of comparison, the amplitude of average torque, electromagnetic torque ripple and cogging torque before and after optimization of different methods are listed in the same table (Table 4).

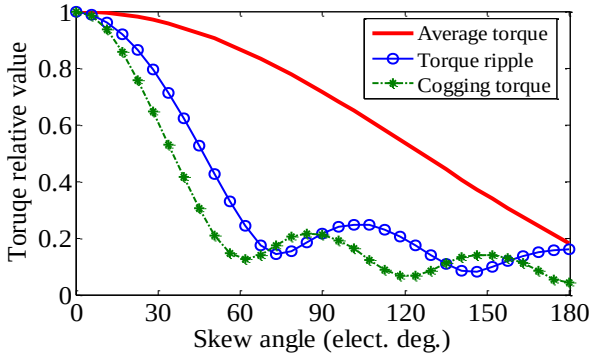

Fig. 11. Torque relative value at different skew angles.

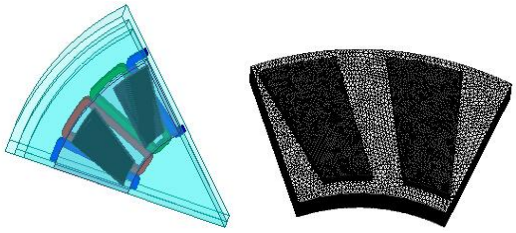

Fig. 12. 3D finite element model of motor after skewing.

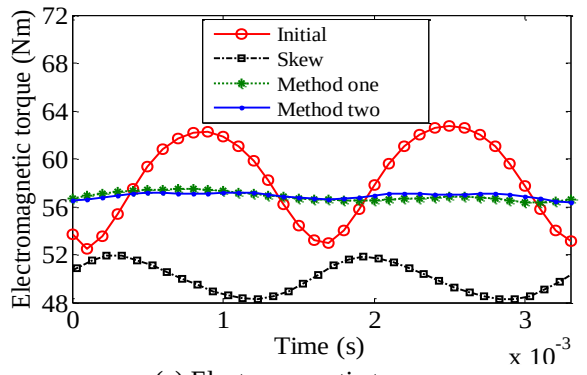

(a) Electromagnetic torque

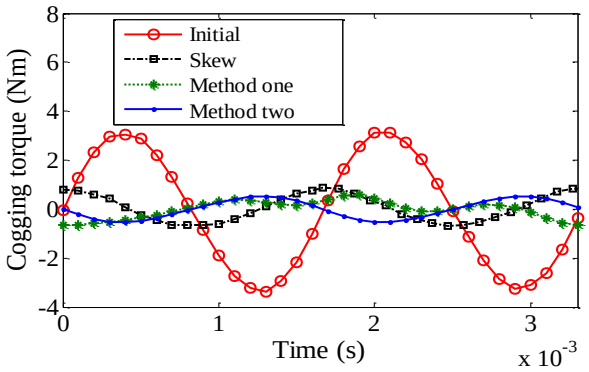

(b) Cogging torque

Fig. 13. Comparison of results by different optimization methods.

Table 4: Results contrast of different optimization methods

	Original	Skew Method	Method One	Method Two
$T_{average}$	57.71 Nm	50.07 Nm	56.80 Nm	57.05 Nm
T_{ripple}	4.71 Nm	1.82 Nm	0.63 Nm	0.58 Nm
T_{cog}	3.13 Nm	0.88 Nm	0.46 Nm	0.43 Nm

From Table 4, we can see that the optimization results of the two proposed methods are almost the same from each other. However, method one will change the spatial distribution of the air gap field and introduce low order magnetic field which may be bad for the vibration and noise. Method two will not change the magnetic field distribution but its magnets have complex structure which will increase the manufacturing cost. So these two methods each has its own advantages and disadvantages. We can make a choice according to the requirement of different application situations.

VI. CONCLUSION

In this paper, two novel techniques for torque optimization in AFPM machines are presented. Their accuracy and validity were verified by 3D FEM. The proposed methods were also compared with skew technique which is popular nowadays. Result showed that the proposed methods can greatly reduce the overall pulsating torque without sacrificing the average torque significantly. Some notable characteristics of the two methods are summarized as follows.

i) By establishing the analytical model of torque, a significant amount of time can be saved during the optimization compared with 3D FEM. This is important in the initial stage of motors design.

ii) Average torque, cogging torque and electromagnetic torque ripple are considered simultaneously in the optimization so it can reduce the overall pulsating torque without decreasing the average torque significantly.

iii) The optimization objectives and constraint conditions can be flexibly adjusted to meet different requests.

As the two proposed methods were only verified by FEM, future work would include manufacturing of prototype and validation of the optimization methods by experimental tests.

ACKNOWLEDGMENT

This work was supported by the National Natural Science Foundation of China (51375343) and the National Major Scientific Instrument Equipment Project of China (2012YQ150256).

REFERENCES

[1] F. G. Capponi, G. D. Donato, and F. Caricchi, "Recent advances in axial-flux permanent-magnet machine technology," *IEEE Trans. Ind. Appl.*, vol. 48, no. 6, pp. 2190-2205, Nov.-Dec. 2012.

[2] M. Aydin and M. Gulec, "Reduction of cogging torque in double-rotor axial-flux permanent-magnet disk motors: A review of cost-effective magnet-skewing techniques with experimental verification," *IEEE Trans. Ind. Electron.*, vol. 61, no. 9, pp. 5025-5034, Sep. 2014.

[3] F. Caricchi, F. G. Capponi, F. Crescimbini, and L. Solero, "Experimental study on reducing cogging torque and no-load power loss in axial-flux permanent-magnet machines with slotted winding," *IEEE Trans. Ind. Appl.*, vol. 40, no. 4, pp. 1066-1075, Jul.-Aug. 2004.

[4] M. Aydin, Z. Q. Zhu, T. A. Lipo, and D. Howe, "Minimization of cogging torque in axial-flux permanent-magnet machines: Design concepts," *IEEE Trans. Magn.*, vol. 43, no. 9, pp. 3614-3622, Sep. 2007.

[5] M. Aydin, "Magnet skew in cogging torque minimization of axial gap permanent magnet motors," in *Proc. 18th Int. Conf. Electr. Mach.*, pp. 1-6, Sep. 2008.

[6] E. Yolacan, E. Ozyurt, and M. Aydin, "Magnet shape optimization of a slotted surface mounted axial gap PM motor for reducing cogging torque," in *Proc. 19th Int. Conf. Electr. Mach.*, pp. 1-6, Sep. 2010.

[7] M. Aydin, R. Qu, and T. A. Lipo, "Cogging torque minimization technique for multiple-rotor, axial-flux, surface-mounted-PM machines: Alternating magnet pole-arcs in facing rotors," in *IEEE Industry Applications Soc. Annu. Meeting*, pp. 555-561, Oct. 2003.

[8] A. B. Letelier, D. A. González, J. A. Tapia, R. Wallace, and M. A. Valenzuela, "Cogging torque reduction in an axial flux PM machine via stator slot displacement and skewing," *IEEE Trans. Ind. Appl.*, vol. 43, no. 3, pp. 685-693, May-Jun. 2007.

[9] D. A. González, J. A. Tapia, and A. B. Letelier, "Design consideration to reduce cogging torque in axial flux permanent-magnet machines," *IEEE Trans. Magn*., vol. 43, no. 8, pp. 3435-3440, Aug. 2007.

[10] C. Hwang, P. Li, F. C. Chuang, C. Liu, and K. Huang, "Optimization for reduction of torque ripple in an axial flux permanent magnet machine," *IEEE Trans. Magn.*, vol. 45, no. 3, pp. 1760-1763, Mar. 2009.

[11] R. Madhavan and B. G. Fernandes, "A novel technique for minimizing torque ripple in axial flux segmented rotor SRM," in *Proc. IEEE Energy Convers. Congr. Expo*., pp. 3383-3390, Sep. 2011.

[12] W. Q. Chu and Z. Q. Zhu, "Investigation of torque ripples in permanent magnet synchronous machines with skewing," *IEEE Trans. Magn.*, vol. 49, no. 3, pp. 1211-1220, Mar. 2013.

[13] M. S. Islam, S. Mir, T. Sebastian, and S. Underwood, "Design considerations of sinusoidally excited permanent-magnet machines for low-torque-ripple applications," *IEEE Trans. Ind. Appl.*, vol. 41, no. 4, pp. 955-962, Jul.-Aug. 2005.

[14] R. Islam, I. Husain, A. Fardoun, and K. McLaughlin, "Permanent-magnet synchronous motor magnet designs with skewing for torque ripple and cogging torque reduction," *IEEE Trans. Ind. Appl.*, vol. 45, no. 1, pp. 152-160, Jan.-Feb. 2009.

[15] S. Jang, H. Park, J. Choi, K. Ko, and S. Lee, "Magnet pole shape design of permanent magnet machine for minimization of torque ripple based on electromagnetic field theory," *IEEE Trans. Magn.*, vol. 47, no. 10, pp. 3586-3589, Oct. 2011.

[16] S. Lee, G. Kang, J. Hur, and B. Kim, "Quasi-zero torque pulsation of surface permanent magnet synchronous motor for ship gyro stabilizer by pole slot number and air-gap designs," *IEEE Trans. Magn.*, vol. 50, no. 2, pp. 1033-1036, Feb. 2014.

[17] F. Scuiller, "Magnet shape optimization to reduce pulsating torque for a five-phase permanent-magnet low-speed machine," *IEEE Trans. Magn.*, vol. 50, no. 4, pp. 3431-3439, Apr. 2014.

[18] T. F. Chan, L. L. Lai, and S. Xie, "Field computation for an axial flux permanent-magnet synchronous generator," *IEEE Trans. Energy Convers*., vol. 24, no. 1, pp. 1-11, Mar. 2009.

[19] Y. J. Zhang, S. L. Ho, H. C. Wong, and G. D. Xie, "Analytical prediction of armature-reaction field in disc-type permanent magnet generators," *IEEE Trans. Energy Convers*., vol. 14, no. 4, pp. 1385-1390, Dec. 1999.

[20] Z. Q. Zhu and D. Howe, "Instantaneous magnetic field distribution in brushless permanent magnet DC motors, Part III: Effect of stator slotting," *IEEE Trans. Magn.*, vol. 29, no. 1, pp. 143-151, Jan. 1993.

[21] P. Virtič, P. Pišek, M. Hadžiselimović, T. Marčič, and B. Štumberger, "Torque analysis of an axial flux permanent magnet synchronous machine by using analytical magnetic field calculation," *IEEE Trans. Magn.*, vol. 45, no. 3, pp. 1036-1039, Mar. 2009.

[22] M. Aydin, S. Huang, and T. A. Lipo, "Torque quality and comparison of internal and external rotor axial flux surface-magnet disc machines," *IEEE Trans. Ind. Electron.*, vol. 53, no. 3, pp. 822-830, Jun. 2006.

Shuanglong Wu a Ph.D. candidate majoring in Vehicle Engineering at Tongji University, Shanghai, China. He received the Bachelor degree of Vehicle Engineering in 2013 from South China University of Technology,Guangzhou, China. His main research interests are in the control of vibration and noise of motor and generator.

Shuguang Zuo a Professor at Tongji University, Shanghai, China. He received the B.S. degree in Mechanical Design from Hunan Agricultural University, Changsha, China, in 1990, and the M.S. and Ph.D. degrees in Automotive Engineering from Jilin University, Changchun, China, in 1993 and 1996, respectively. From 1996 to 1998, he was a Postdoctoral Researcher with the Aviation and Aerospace Technology Postdoctoral Research Station, Nanjing Aeronautics and Astronautics University, Nanjing, China. He is now a Professor with the College of Automotive Engineering, Tongji University. His research interests include vehicle system dynamics and control, vehicle vibration and noise control, and vibration and noise of electrical machines.